View Article Online / Journal Homepage / Table of Contents for this issue

JAAS

Journal of Analytical Atomic Spectrometry

www.rsc.org/jaas

Volume 24 | Number 9 | September 2009 | Pages 1129–1276

Published on 27 April 2009. Downloaded by Michigan State University on 23/01/2016 09:10:25.

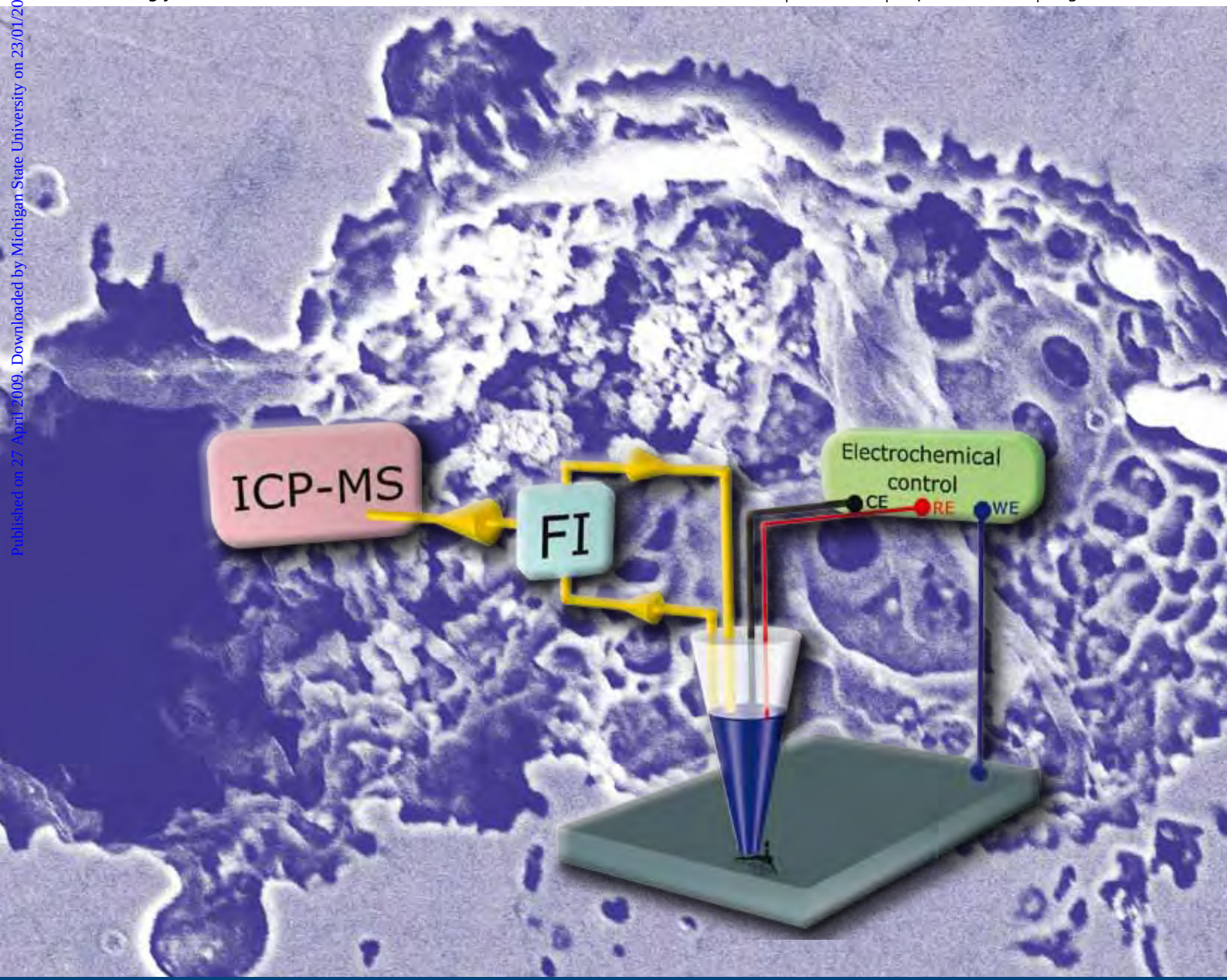

Themed Issue 2008 Asia-Pacific Winter Conference on Plasma Spectrochemistry

ISSN 0267-9477

RSC Publishing

Editorial
Furuta
2008 Third Asia-Pacific Winter Conference on Plasma Spectrochemistry, Tsukuba, Japan, November 16–21

Hot Paper
Homazava *et al.*
Online hyphenation of potentiostat to a microflow-capillary FI-ICP-MS for characterization of local corrosion processes

0267-9477(2009)24:9;1-L

View Article Online

Online hyphenation of potentiostat to a microflow-capillary FI-ICP-MS for simultaneous *in situ* electrochemical, time and element resolved characterization of local corrosion processes—an application for Zr-bulk metallic glass†

Nadzeya Homazava,*[ab] Thomas Suter,[c] Patrik Schmutz,[c] Sven Toggweiler,[d] Ansgar Grimberg,[e] Urs Krähenbühl[b] and Andrea Ulrich[a]

Received 20th January 2009, Accepted 9th April 2009
First published as an Advance Article on the web 27th April 2009
DOI: 10.1039/b901077g

Published on 27 April 2009. Downloaded by Michigan State University on 23/01/2016 09:10:25.

A novel technique based on an online hyphenation of an electrochemical control to a microflow-capillary FI-ICP-MS set-up is developed for the local investigation of corrosion processes. Construction and analytical optimization steps are presented in detail. The novel microflow-capillary FI-ICP-MS technique with simultaneous electrochemical control enables acquisition of electrochemical and chemical element-resolved data at the same time. Precise characterization of the local dissolution corrosion processes is achieved with the new technique. The capabilities of the new hyphenated technique are demonstrated for the example of zirconium bulk metallic glasses, which are prospective materials for various industrial applications. The corrosion susceptibility of $Zr_{58.5}Cu_{15.6}Ni_{12.8}Al_{10.3}Nb_{2.8}$ in 0.1 M HCl, 0.1 M NaCl and 0.001 M NaCl was evaluated at open circuit potential and during electrochemical potentiodynamic polarization of the sample surface. A preferential release of less noble elements like Ni and Al from bulk metallic glass was revealed, whereas the dissolution of Cu from the material was strongly hindered.

Introduction

Plasma spectrochemistry methods, especially inductively coupled plasma mass spectrometry (ICP-MS), have gained an increasing interest in corrosion related investigations over the past ten years. Characteristics like fast multi-element detection capability, high sensitivity and low detection limits provide excellent possibilities for simultaneous multi-element monitoring of dissolution processes during corrosion.[1,2]

ICP-MS is suitable for corrosion dissolution studies both on oxide covered passive materials, *e.g.* titanium[3,4] or CoCr alloys[4] for biomedical applications, and on actively dissolving materials *e.g.* wolfram-carbide-cobalt material (WC-Co).[5] Most chemical analyses have been performed as bulk solution immersion tests, but also a continuous flow analysis has been described by Ogle *et al.*, who demonstrated capabilities of a flow cell ICP optical emission spectroscopy (ICP-OES) technique to detect elementary dissolution rates during corrosion of various materials.[6–8] Most recently, a similarly constructed flow cell coupled to ICP-MS was applied to corrosion investigations and potentiodynamic polarization of WC-Co material by Hochstrasser-Kurz *et al.*[9]

However, local- and time-resolved, element-specific data on corrosion processes are required to investigate the initial corrosion steps and corrosion mechanisms especially in the case of localized corrosion processes. Therefore, a novel analytical microflow-capillary has been developed at Empa[2,10,11] for coupling to ICP-MS. The idea to use a micro-capillary concept for the investigation of local corrosion processes is related to an electrochemical set-up with a static microcapillary developed by T. Suter.[12]

However, the here described novel dynamic microflow-capillary is especially designed for local online corrosion experiments and enables a continuous medium circulation over the material of interest. The microcapillary is filled with a corrosive medium and placed on a distinct spot of the material. Online hyphenation of the microflow-capillary *via* flow injection (FI) allows transient sampling and corrosion sample introduction to the ICP-MS. It offers significant advantages over conventional sample introduction due to an excellent matrix tolerance even at a high level of total dissolved salt concentrations (*e.g.* 0.1 M–1 M NaCl) and minimization of the required sample volumes. The later improves detection limits, because the equivalent detection limits in ng cm^{-2} are calculated from the detection limits in ng L^{-1} according to the equation: $DL_{ng\ cm^{-2}} = DL_{ng\ L^{-1}} \cdot V/S$, where V is the liquid volume in the capillary and S is the area of the sample surface exposed to the corrosion attack. Thus, the minimization of the sample volumes possible in FI-ICP-MS leads to the minimization of the equivalent

[a]*Empa, Swiss Federal Laboratories for Materials Testing and Research, Laboratory for Analytical Chemistry, Ueberlandstrasse 129, CH-8600 Duebendorf, Switzerland. E-mail: nadzeya.homazava@empa.ch; Fax: +41 44 823 4041; Tel: +41 44 823 4354*
[b]*University of Bern, Department for Chemistry and Biochemistry, Freiestrasse 3, CH-3012 Bern, Switzerland*
[c]*Empa, Swiss Federal Laboratories for Materials Testing and Research, Laboratory for Corrosion and Materials Integrity, Ueberlandstrasse 129, CH-8600 Duebendorf, Switzerland*
[d]*Empa, Swiss Federal Laboratories for Materials Testing and Research, Solid State Chemistry and Catalysis, Ueberlandstrasse 129, CH-8600 Duebendorf, Switzerland*
[e]*University of Bern, Institute of Physics, Sidlerstrasse 5, CH-3012 Bern, Switzerland*
† Presented at the Third Asia-Pacific Winter Conference on Plasma Spectrochemistry, Tsukuba, Japan, November 16–21, 2008.

View Article Online

Published on 27 April 2009. Downloaded by Michigan State University on 23/01/2016 09:10:25.

detection limits. Moreover, due to a small diameter of the capillary opening down to a width of 250 μm, the analyzed area of the corrosion attack can be significantly decreased.

So far, only measurements at open circuit potential were available with the microflow-capillary FI-ICP-MS set-up. In this study, a hyphenation of an electrochemical control to the microflow-capillary FI-ICP-MS set-up is presented, allowing simultaneous online ICP-MS and electrochemical data monitoring during the corrosion process. As already mentioned above, a static micro-capillary in combination with a 3 electrode electrochemical control concept was developed by Suter *et al.* and applicability and advantages of this technique in corrosion investigations were demonstrated in various applications.[12–15] The static micro-capillary-electrochemical system allows investigations of localized corrosion processes even down to the upper nm range. However, it provides an electrochemical corrosion characterization only.

Additional adaptation of an electrochemical control to the microflow-capillary-FI-ICP-MS set-up combines the electrochemical idea of T. Suter *et al.* and our idea of localized investigations on element-specific dissolution processes. This opens new possibilities in corrosion studies by enabling simultaneous electrochemical and element-specific data acquisition. The idea is realized using the investigated sample as the working electrode, while the reference and counter micro-electrodes are installed into the microflow-capillary.

The efficiency of the novel hyphenated technique is verified by a corrosion study on Zr-bulk metallic glass (Zr-BMG) with the composition of $Zr_{58.5}Cu_{15.6}Ni_{12.8}Al_{10.3}Nb_{2.8}$. Zr-BMGs have been developed as materials with prominent physical properties like high strength and low Young's modulus.[16,17] Moreover, electrochemical investigations performed on different Zr-BMGs revealed their high uniform corrosion resistance.[18–21] Thus, they are highly promising for various industrial and biomedical applications. As an unconventional application Zr-BMG was used as a collection target for solar wind noble gases on NASAs Genesis mission because of its good etching behaviour and noble gas trapping capabilities.[22]

Recently, we have investigated element-resolved dissolution behaviour of $Zr_{58.5}Cu_{15.6}Ni_{12.8}Al_{10.3}Nb_{2.8}$ with the microflow-capillary FI-ICP-MS at open circuit potential only.[23] However, the new microflow-capillary FI-ICP-MS set-up with a hyphenated electrochemical control allows the simultaneous characterization of the Zr-BMG corrosion behaviour with both element-specific and electrochemical techniques, which is so far not accessible in the literature. Additionally, the Zr-BMG surface before and after corrosion attack was characterized by scanning electron microscopy with energy dispersive X-ray spectrometry (SEM-EDX).

Experimental

Microflow-capillary FI-ICP-MS set-up

Detailed descriptions of the microflow-capillary and the set-up coupling to ICP-MS *via* FI, including the construction and optimization procedures, are given in previous publications.[2,10] The microflow-capillary used in the presented study has an internal diameter of 800 μm. The electrolyte inside the microflow-capillary was pumped with a cycling flow rate of 500 μl min^{-1}. The total cycling volume of the electrolyte was equal to 620 μl, whereas aliquots of 20 μl only were transiently introduced into ICP-MS using a small flow injection loop. The elements released from the material during corrosion were detected online using a quadrupole inductively coupled plasma mass spectrometer ICP-QMS ELAN 6000 (Perkin Elmer/Sciex). The details of the instrument operation conditions are presented in Table 1. The online ICP-MS analysis was performed every 115 s during the potentiodynamic polarization of the sample.

Table 1 ICP-QMS instrument operation conditions

Parameter (unit)	Set point
Analytical instrument	ICP-QMS ELAN 6000
Sample introduction system	Micromist nebulizer MMN 100 with Cinnabar spray chamber
Sampling and skimmer cones	Nickel
Plasma parameters	
Rf Power (W)	1100
Plasma gas flow-rate (L min^{-1})	15
Auxiliary gas flow-rate (L min^{-1})	1
Nebulizer gas flow-rate (L min^{-1})	0.96
Data acquisition parameters	
Dwell time (ms)	30
Readings per replicate	250
Number of replicates	15–20
Analytes monitored	$^{27}Al^+$, $^{60}Ni^+$, $^{65}Cu^+$, $^{90}Zr^+$, $^{93}Nb^+$

Potentiodynamic polarization measurements

To achieve a simultaneous acquisition of the ICP-MS and potentiodynamic polarization data a high resolution, low noise measuring system was coupled to the microflow-capillary FI-ICP-MS set-up. A modified low-noise battery operated potentiostat (Jaissle 1002T-NC-3) was used for the electrochemical measurements. The input resistance was better than 10^{15} Ω and the input current about 10^{-14} A (20 °C). In combination with a good shielding, corrosion currents as low as 10 fA (10^{-14} A) could be detected. A three electrode cell concept with a silver/silver chloride (Ag/AgCl) reference electrode (Dri-Ref™ 450, World Precision Instruments, Sarasota, FL, USA) and a platinum wire (99.95%, World Precision Instruments, Sarasota, FL, USA) as counter electrode was used. The sample served as a working electrode. The reference and counter electrodes were inserted into the microflow-capillary. Fig. 1 schematically shows an adaptation of the electrochemical control to the microflow-capillary FI-ICP-MS set-up.

Since the physical dimensions of the electrodes installed inside the capillary are critical, electrodes with smallest diameters available were implemented. The Pt wire had a diameter of 250 μm, whereas the diameter of the reference micro-electrode tip was 450 μm. Prior to the installation, the electrodes were leached in 1 M hydrochloric acid to minimize a contamination of the corrosive medium. The potentiodynamic polarization measurements were operated with a scanning rate of 0.5 mV s^{-1} from −400 mV to +1000 mV (*vs* Ag/AgCl) after initial immersion at open circuit potential for 5 min. Simultaneously ICP-MS data was acquired every 115 s.

SEM-EDX

The surface of the freshly polished sample before corrosion attack and the corroded sample after the anodic polarization up to +1000 mV (*vs* Ag/AgCl) was studied using a Hitachi S-4800

 This journal is © The Royal Society of Chemistry 2009

View Article Online

Published on 27 April 2009. Downloaded by Michigan State University on 23/01/2016 09:10:25.

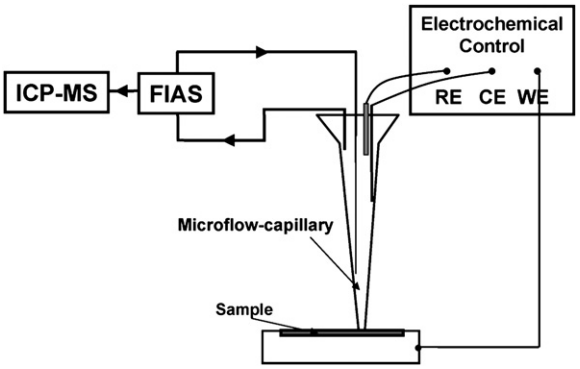

Fig. 1 Scheme of an adaptation of the electrochemical control to the microflow-capillary FI-ICP-MS set-up (RE – reference electrode; CE – counter electrode; WE – working electrode).

scanning electron microscope (SEM) equipped with an Oxford energy dispersive X-ray spectrometer (EDX). The SEM images were recorded using 5 to 10 kV electron beam energy and a sample distance of 8 mm.

Materials and chemicals

The Zr-BMG investigated had a composition of $Zr_{58.5}Cu_{15.6}Ni_{12.8}Al_{10.3}Nb_{2.8}$. The sample was first ground with a SiC paper down to 4000 grit and then polished with a diamond paste down to 1 μm. The surface of the polished sample was cleaned in an ultrasonic bath with absolute ethanol (99.8%, pro analysis quality, Merck, Germany). All corrosion investigations were performed on a freshly polished sample at room temperature.

The following solutions were used as corrosive media: 0.1 M HCl, 0.1 M NaCl and 0.001 M NaCl. The 0.1 M HCl solution was prepared from concentrated hydrochloric acid of ultrapure quality (Merck, Germany). The 0.1 M and 0.001 M NaCl solutions were prepared from sodium chloride of suprapure quality (99.99%, Merck, Germany).

Single element stock solutions of Zr, Nb, Cu, Al and Ni of ICP-MS quality (1 mg L^{-1}, Merck, Germany) were step-wise diluted to prepare single element standard solutions for calibration. The ICP-MS calibration procedure was performed using the mentioned single element standard solutions with matrix matching due to the applied corrosion media, *i.e.* each standard solution contained 0.1 M HCl, 0.1 M NaCl or 0.001 M NaCl as a matrix. The calibration was performed by flow injection, using the same volumes of standard solutions as for the samples. Raw data acquired in the intensity *vs* time mode were exported to Origin 6.1G software (OriginLab Corporation, MA, USA) and smoothed with 11-point Savitzky–Golay moving window. The calculations were done using peak height data. The background subtraction from peak profile was systematically performed based on 5-baseline readings prior to the peak acquirement.

Results and discussion

Hyphenation of the potentiostat to the microflow-capillary FI-ICP-MS set-up. Analytical optimization procedure

To allow simultaneous electrochemical and element-resolved data acquisition during corrosion of the Zr-BMG, a potentiostat was coupled to the microflow-capillary FI-ICP-MS set-up. The Zr-BMG was connected to the potentiostat instrument as a working electrode. Pt-wire and Ag/AgCl electrodes were inserted into the microcapillary as counter and reference electrodes, respectively.

The counter electrode (CE) and reference electrode (RE) have to fulfil the following criteria to be appropriate for use in the current microflow-capillary set-up:

a) to be equipped with the smallest electrode dimensions;

b) to provide minimal contamination levels to the corrosive medium.

Both electrodes were preliminary leached in the different relevant corrosion media solutions to estimate the possible contamination levels, which may originate from the electrodes. Fig. 2A shows the results of the static RE and CE leach-out in 0.1 M NaCl, 0.1 M HCl and 1 M HCl. The electrodes were immersed in the mentioned solutions for 3 h; the solutions were later analyzed with ICP-MS. Fig. 2B demonstrates the results of the dynamic leaching of the RE and CE together in 1 M HCl. In this case the electrodes were inserted into the capillary filled with 1 M HCl solution, which was pumped with a cycling flow of 500 μl min^{-1} for 2 h according to the subsequent corrosion experiments. The same elements as in the static leaching were monitored. However, only for the elements Al, Mg, and Zn have significant signals been detected.

As it can be concluded from Fig. 2A and Fig. 2B the highest contamination levels were detected for Al and Mg at levels of 1–3 μg L^{-1}. The increased signal level for Cr in HCl solution originating from $ArCl^+$ spectral interferences was compensated by matrix matching of blank solution and standards.

To avoid contamination of corrosive media used in the corrosion experiments, both electrodes were preliminary leached in 1 M HCl for 3 hours and several times rinsed with ultra-pure Milli-Q water before they were installed into the microflow-capillary. During the first 5 min of the corrosion investigation, the ICP-MS background signal was monitored at open circuit potential. Later on it was used as a blank level for the procedure of the ICP-MS signal calculation.

The detection limits of the technique for the elements of interest $^{27}Al^+$, $^{60}Ni^+$, $^{65}Cu^+$, $^{90}Zr^+$ and $^{93}Nb^+$ were estimated on a level of ng L^{-1} and are published elsewhere.[23] Each corrosion investigation was repeated three times at random spots of the Zr-BMG sample. The standard deviations (SDs) of the element concentration determination, originating from the ICP-MS analysis were much lower compared to the SDs of the determined element concentrations originating from these triple determinations at different spots. Hence, the precision of the technique is limited by the SDs of the multiple determinations. Moreover, the ICP-MS data acquired in the measurements are corrected for the value of the pitting potential (E_{pit}, electrochemical data) for each measurement.

Fig. 3 shows an exemplary procedure of the ICP-MS Zr data correction for E_{pit} for three independent corrosion measurements in 0.1 M NaCl. A comparison of Fig. 3A and Fig. 3B reveals that the mentioned correction procedure leads to final data with increased precision. Pitting potential is determined from the potentiodynamic polarization curve (Fig. 4) as the potential at which the current (current density) starts to increase sharply with the further increase of the potential.

View Article Online

Published on 27 April 2009. Downloaded by Michigan State University on 23/01/2016 09:10:25.

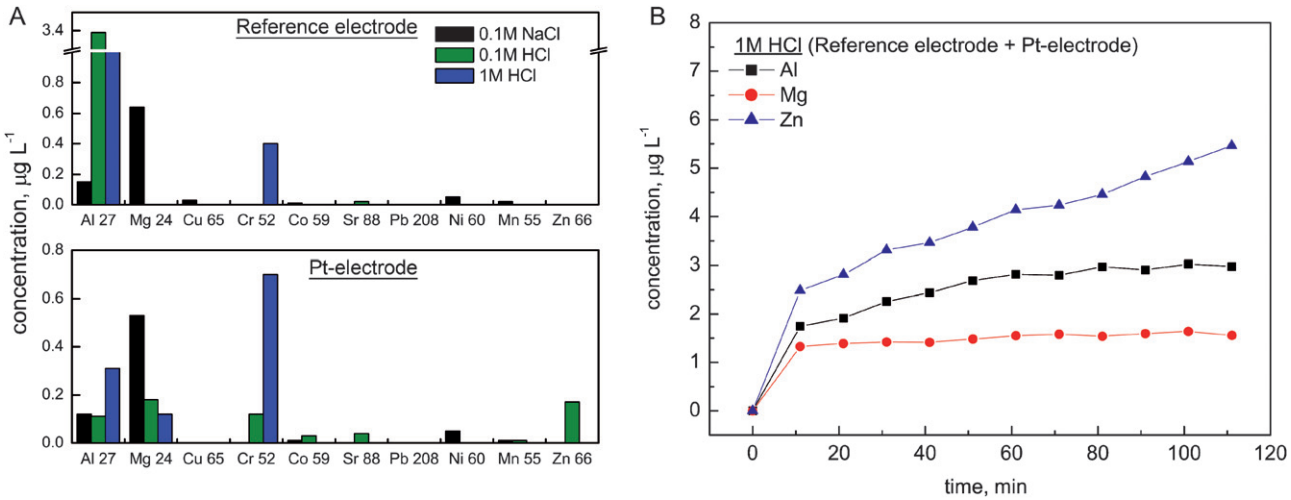

Fig. 2 **A.** Elemental concentrations in 0.1 M NaCl, 0.1 M HCl and 1 M HCl solutions after the static leaching procedure of Pt-electrode and Ag/AgCl Dri-Ref™ reference electrodes; **B.** Elemental concentrations in 1 M HCl solution after dynamic leaching of Pt-electrode and Ag/AgCl Dri-Ref™ reference electrode together.

Corrosion study on $Zr_{58.5}Cu_{15.6}Ni_{12.8}Al_{10.3}Nb_{2.8}$. Potentiodynamic polarization

Potentiodynamic polarization curves obtained for $Zr_{58.5}Cu_{15.6}Ni_{12.8}Al_{10.3}Nb_{2.8}$ in 0.1 M NaCl, 0.001 M NaCl and 0.1 M HCl are shown in Fig. 4.

The open circuit potential (E_{ocp}) and the pitting potential (E_{pit}) shift towards more negative values, when the acidity of the corrosive medium or the chloride concentration is increased.

These results are in the following ranking:

$$E_{pit}\ (0.1\ M\ HCl) < E_{pit}\ (0.1\ M\ NaCl) < E_{pit}\ (0.001\ M\ NaCl).$$

The polarization curve of Zr-BMG in 0.001 M NaCl is characterized by the presence of a wide passive region, $\Delta E = E_{pit} - E_{ocp} = 285$ mV (*vs* Ag/AgCl), whereas for a higher chloride concentration the passive region is much more narrow, $\Delta E = 71$ mV (*vs* Ag/AgCl) for 0.1 M NaCl. In 0.1 M HCl, there is a first region of $\Delta E = 50$ mV (*vs* Ag/AgCl) with lower dissolution rate, but no real passivation is observed.

$Zr_{58.5}Cu_{15.6}Ni_{12.8}Al_{10.3}Nb_{2.8}$ exhibits a high uniform corrosion resistance indicated by low values of passive current density on a level of 10^{-7}–10^{-6} A cm^{-2} for the corrosive media tested in the neutral pH domain. However, during anodic polarization in chloride containing solutions, the Zr-BMG is

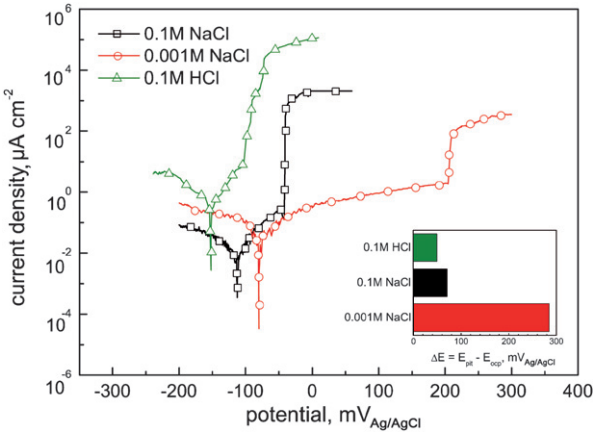

Fig. 4 Potentiodynamic polarization curves of $Zr_{58.5}Cu_{15.6}Ni_{12.8}Al_{10.3}Nb_{2.8}$ in 0.1 M NaCl, 0.001 M NaCl and 0.1 M HCl.

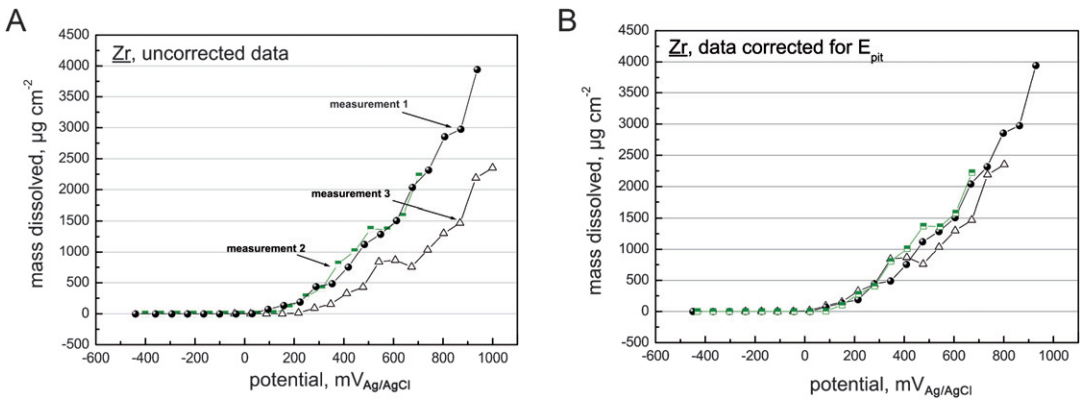

Fig. 3 Correction of the ICP-MS measurements according to different values of E_{pit} for 3 independent corrosion measurements of Zr in 0.1 M NaCl: **A.** Non-corrected data; **B.** Corrected data.

 This journal is © The Royal Society of Chemistry 2009

View Article Online

Published on 27 April 2009. Downloaded by Michigan State University on 23/01/2016 09:10:25.

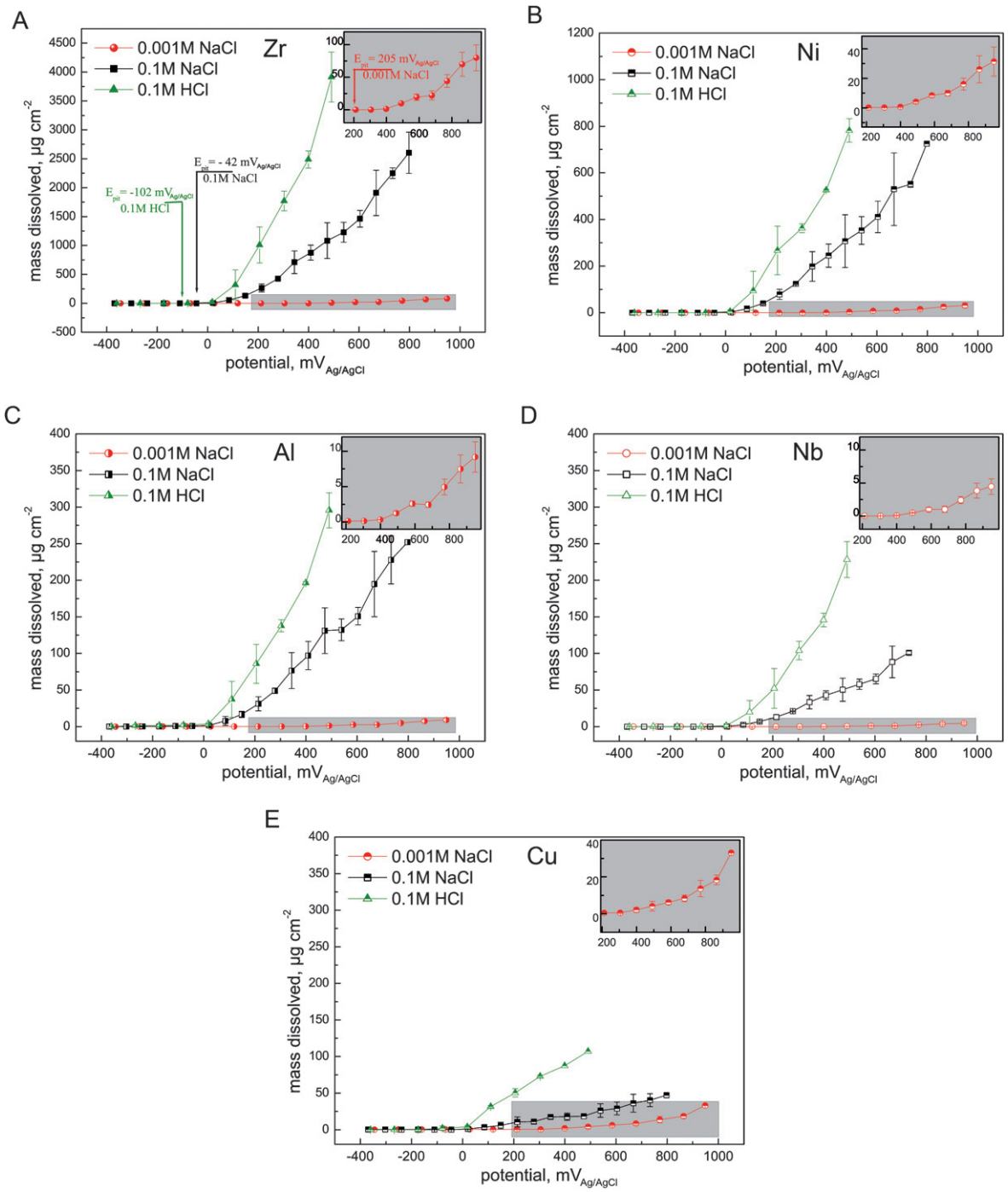

Fig. 5 Dissolution behaviour of $Zr_{58.5}Cu_{15.6}Ni_{12.8}Al_{10.3}Nb_{2.8}$ constituent elements upon potentiodynamic polarization: **A.** zirconium Zr; **B.** nickel Ni; **C.** aluminium Al; **D.** niobium Nb; **E.** copper Cu. Error bars indicate the standard deviations for $n = 3$.

highly prone to localized (pitting) corrosion. These findings are consistent with electrochemical results previously published for Zr-BMGs of other compositions.[24,25]

Based on the potentiodynamic polarization data, conclusions on the corrosion resistance or susceptibility of Zr-BMG can be made. However, an important additional element-resolved characterization of Zr-BMG corrosion dissolution behaviour is only accessible using the novel potentiostat hyphenated micro-flow-capillary FI-ICP-MS set-up.

Corrosion study on $Zr_{58.5}Cu_{15.6}Ni_{12.8}Al_{10.3}Nb_{2.8}$. Element- and time resolved online dissolution behaviour monitored with FI-ICP-MS technique under electrochemical control

Fig. 5A–E shows the measured elemental dissolution rates of $Zr_{58.5}Cu_{15.6}Ni_{12.8}Al_{10.3}Nb_{2.8}$ in 0.1 M NaCl, 0.001 M NaCl and 0.1 M HCl at different potentials achieved during the potentiodynamic polarization of the sample. For all elements monitored with ICP-MS the dissolution curve can be easily divided into two regions before and after pitting potential. The values of the pitting

View Article Online

Published on 27 April 2009. Downloaded by Michigan State University on 23/01/2016 09:10:25.

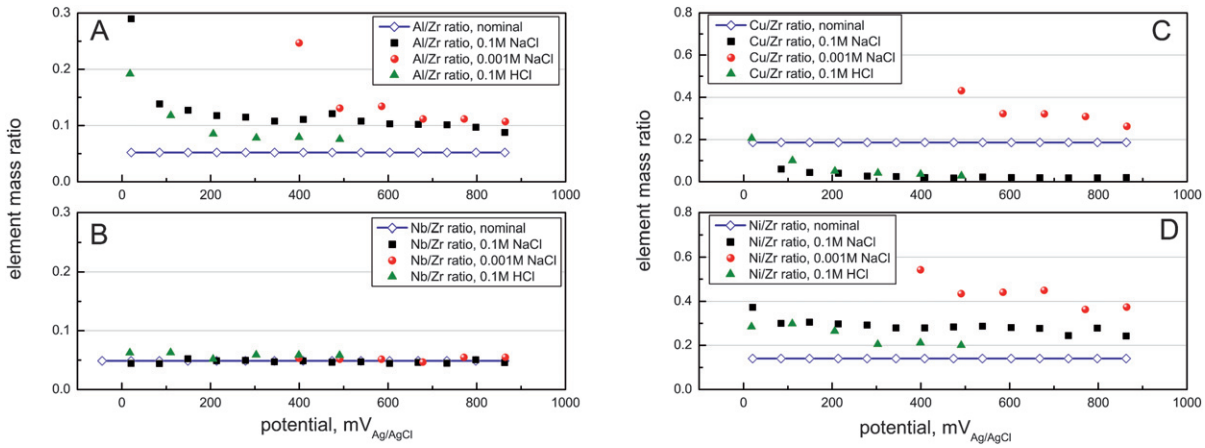

Fig. 6 The dependence of the mass ratio of elements dissolved in 0.1 M HCl, 0.1 M NaCl and 0.001 M NaCl compared to the nominal mass ratio of elements derived from the Zr-BMG composition: **A.** Al/Zr; **B.** Nb/Zr; **C.** Cu/Zr; **D.** Ni/Zr.

potentials in 0.1 M NaCl, 0.001 M NaCl and 0.1 M HCl are exemplary marked on the Zr-dissolution curve (Fig. 5A). Before the pitting potential is reached, only very low Al and Cu concentrations in the range of 20 to 60 ng cm^{-2} are detected for all investigated corrosion media. For the elements Zr, Nb and Ni, the ICP-MS signals remain almost at background level until the potentiodynamic polarization scan reaches the pitting potential value. The low concentrations of Al and Cu are already detected during cathodic prepolarization of the sample and at open circuit potential immersion prior the anodic polarization, *e.g.* at potentials from −400 to −100 mV (*vs* Ag/AgCl). Thus, the initial process of Al and Cu release from the Zr-BMG into corrosive solution can be explained as a process of chemical dissolution of the natural oxide film, when alkanisation of the solution at the surface occurs as a result of cathodic reduction. Natural oxide films (called passive films) are usually formed on top of the bulk metallic glasses at ambient air and have a typical thickness of 5–10 nm.[26] A similar mechanism of Zr-BMG oxide film dissolution at open circuit potential was proposed in our previous publication.[23]

As the potentiodynamic polarization curve passes through the value of E_{pit} a massive release of all elements is detected online with ICP-MS. The steepness of the dissolution curve decreases in the following order 0.1 M HCl > 0.1 M NaCl > 0.001 M NaCl, confirming the electrochemical data of $Zr_{58.5}Cu_{15.6}Ni_{12.8}Al_{10.3}Nb_{2.8}$ corrosion susceptibility.

The absolute amount of Zr released in 0.1 M HCl and 0.1 M NaCl is estimated in the range of mg cm^{-2}, whereas for all other elements the amount of species dissolved is in the range of μg cm^{-2}. Generally, the amount of species released in 0.1 M HCl is 3 to 5 times higher than in 0.1 M NaCl. The dissolution behaviour in the lower chloride concentrated 0.001 M NaCl is characterized by significantly reduced dissolution rates. On average the dissolved mass is 30 to 40 times lower than in 0.1 M NaCl. The trends are also consistent with the limiting current density measured electrochemically that are much higher for HCl than for the NaCl solution.

The element-resolved dissolution rates for $Zr_{58.5}Cu_{15.6}Ni_{12.8}Al_{10.3}Nb_{2.8}$ decrease in the following order, based on the data shown in Fig. 5A to Fig. 5E: Zr > Ni > Al > Nb > Cu.

Comparing this data set to the mass composition of the BMG material (70.06% Zr, 13.01% Cu, 9.86% Ni, 3.65% Al, and 3.42% Nb) it can be concluded that:

a) the release of all elements with the exception of Cu is in agreement with the composition of the bulk metallic glass;

b) the release of Cu from $Zr_{58.5}Cu_{15.6}Ni_{12.8}Al_{10.3}Nb_{2.8}$ is strongly inhibited.

The dependence of the mass ratio of elements dissolved in 0.1 M HCl, 0.1 M NaCl and 0.001 M NaCl compared to the nominal mass ratio of elements derived from the Zr-BMG composition is shown in Fig. 6A to Fig. 6D. Fig. 6A and Fig. 6D indicate preferential Al and Ni dissolution, characterized by two times higher mass ratios of Al to Zr and Ni to Zr dissolved from the material compared to the nominal composition ratios in all corrosive media.

Nb and Zr are released very close to the nominal ratio in 0.1 M HCl, 0.1 M NaCl and 0.001 M NaCl, indicating that the dissolution of Zr and Nb proceeds in accordance with the material composition (Fig. 6B). The ratio of Cu to Zr dissolved from the material is strongly reduced especially in the high chloride concentrated solutions (0.1 M HCl and 0.1 M NaCl), whereas for 0.001 M NaCl an enhanced Cu/Zr ratio is detected (Fig. 6C). It is important to point out that only a relative enhancement of the Cu/Zr ratio in 0.001 M NaCl is observed, the absolute amount of copper dissolved from the material follows the same sequence as for the other elements:

0.1 M HCl > 0.1 M NaCl > 0.001 M NaCl.

The following explanation of the observed data is proposed. The elements of the Zr-BMG are characterized by standard electrode potentials: E° (Zr^{4+}/Zr) = −1.45 V (*vs* SCE); E° (Nb^{3+}/Nb) = −1.099 V (*vs* SCE); E° (Al^{3+}/Al) = −1.662 V (*vs* SCE); E° (Ni^{2+}/Ni) = −0.257 V (*vs* SCE); E° (Cu^{2+}/Cu) = +0.342 V (*vs* SCE).[27] Thus, the active dissolution processes for all elements, with the exception of Cu, can be expected after oxide film breakdown and as soon as the E_{pit} is reached. However, the standard electrode potential is related to the binding energy of a compound, meaning that for a Zr-BMG comparison of single elements data is only indicative. The increased dissolution rates of Al and Ni compared to Nb and Zr can be interpreted if the solubility of the corrosion products is taken into account. Nb chloride has a low solubility in both neutral and acidic aqueous

 This journal is © The Royal Society of Chemistry 2009

View Article Online

Published on 27 April 2009. Downloaded by Michigan State University on 23/01/2016 09:10:25.

solutions and tends to be a fast hydrolysis process, which can be described as follows:

$$NbCl_5 + xH_2O \rightarrow Nb(OH)_xCl_{5-x} + xH^+ + xCl^- \quad (1)$$

At chloride concentrations lower than 2 M a formation of a flocculent precipitate of $Nb(OH)_3Cl_2$ and/or $Nb(OH)_5$ occurs.[28]

Zr chloride is also characterized by a low solubility in neutral and weak acidic aqueous solutions, resulting in a similar hydrolysis process:[29]

$$Zr^{4+} + xH_2O \rightarrow Zr(OH)_x^{(4-x)+} + xH^+ \quad (2)$$

Hence, the precipitation of Zr and Nb hydrolyzed corrosion products is expected in the studied corrosive media. On the other hand, Al and Ni chlorides have a high solubility in both neutral and acidic solutions. Therefore, an enhanced dissolution of Al and Ni compared to Zr and Nb is explainable by the different solubility products of these elements.

Due to the highest standard electrode potential of Cu ($E^\circ(Cu^{2+}/Cu) = +0.342$ V (*vs* SCE)) among all elements in $Zr_{58.5}Cu_{15.6}Ni_{12.8}Al_{10.3}Nb_{2.8}$, a noble behaviour of Cu is expected and the lowest dissolution rate for Cu is reasonable. But here again, first, preferential dissolution steps need to occur, to be able to speak of pure copper dissolution.

Futhermore, the increased ratio of Cu/Zr release in 0.001 M NaCl is yet not fully understood. However, studies of localized corrosion behaviour of copper indicate that its susceptibility and dissolution is influenced by the formation of poorly soluble CuCl compounds. The precipitate can only form in the presence of a large amount of chloride, and this supports the fact that highest susceptibility to localized corrosion for copper is found for 0.001 M NaCl.[30] Localized corrosion of copper however only occurs at pH's above 8 so that the explanation needs to be investigated in more detail. However, dealloying and copper remnant are often found, when copper containing compounds are considered.[31]

To discuss the data presented in this paper, the morphology of the pits formed on the surface of Zr-BMG after anodic polarization up to +1000 mV (*vs* Ag/AgCl) was studied with SEM-EDX and are provided in Fig. 7A and Fig. 7B. Both figures show overviews of the corroded area, pits growth occurred in the area where the capillary was placed (a dark circle with a radius of about 400 μm). Detailed images of the pits formed in 0.1 M HCl and 0.1 M NaCl are shown in Fig. 7C and Fig. 7D, respectively. It is clearly visible that the number and the pit size are highest in 0.1 M HCl.

Remarkable is the shape of the corrosion attack at the Zr-BMG surface, which appears in the form of a circle of about 800 μm, whereas the inner region seems to be less attacked. The exact reason for this phenomenon is not yet understood. A possible explanation might be a local enhancement of acidity or

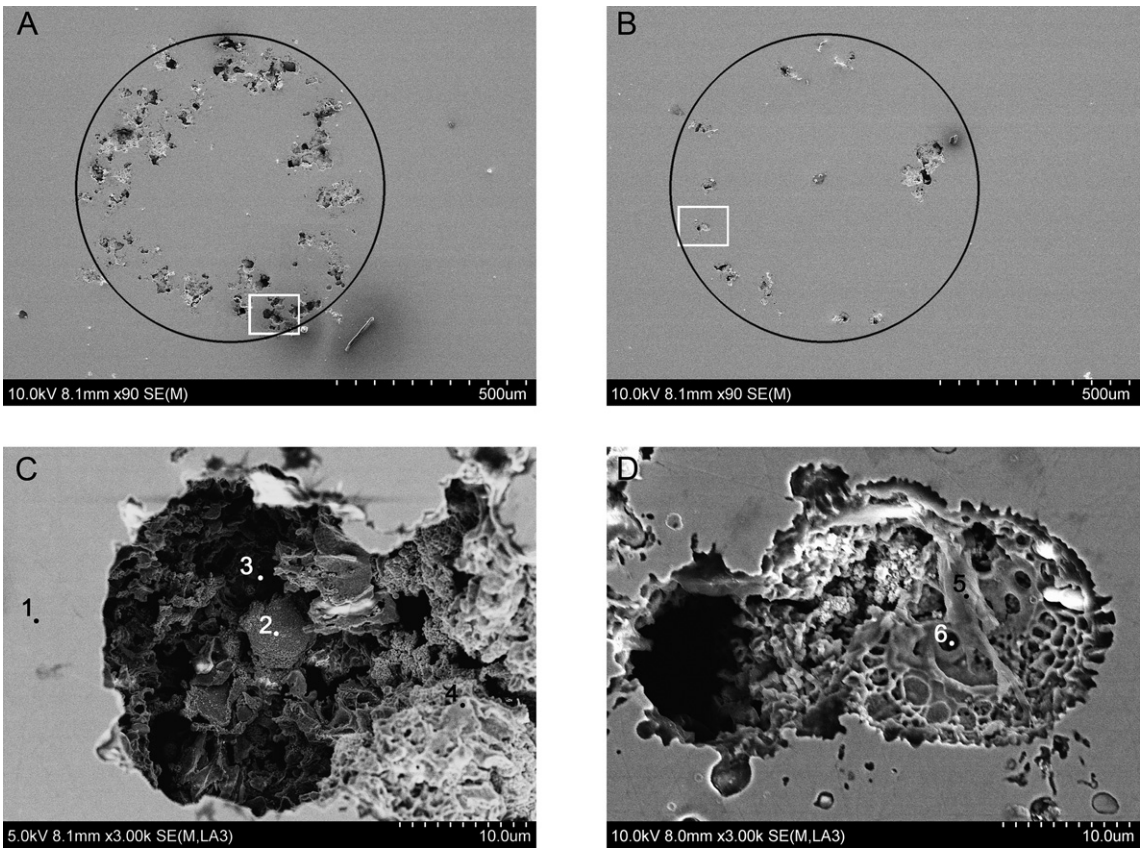

Fig. 7 SEM images of the corroded surface of Zr-BMG after potentiodynamic polarization up to +1000 mV (*vs* Ag/AgCl) in: **A.** 0.1 M HCl; **B.** 0.1 M NaCl. SEM images of the pits on the surface of Zr-BMG in: **C.** 0.1 M HCl (enlarged section of Fig. 7A); **D.** 0.1 M NaCl (enlarged section of Fig. 7B). The numbered points indicate the spots, where the EDX analysis is performed.

View Article Online

Published on 27 April 2009. Downloaded by Michigan State University on 23/01/2016 09:10:25.

Table 2 Mass concentrations of elements in numbered spots (Fig. 7) derived from EDX analysis at the marked points in the Fig. 7C and Fig. 7D

	O	Al	Ni	Cu	Zr	Nb
Nominal composition	—	3.65	9.86	13.01	70.06	3.42
Point 1	—	3.6	8.8	12.9	74.7	—
Point 2	—	—	—	**86.0**	**14.0**	—
Point 3	—	—	—	**83.9**	**16.1**	—
Point 4	6.8	2.0	8.8	29.8	52.6	—
Point 5	11.4	—	13.0	41.3	34.3	—
Point 6	—	—	**17.2**	**67.3**	**15.5**	

chloride concentration at the outer region, caused by less well mixing zones and diffusion problems due to the capillary geometry or crevices under the capillary. This can obviously play a role when fast active dissolution takes place, but in the presented case also the corrosion initiation is dependent on the location. This observation also points to another possible cause, which is the pressure applied on the surface by the capillary and which is higher close to the capillary walls than in the middle of the exposed area. Induced stress has to be taken into account when the susceptibility to localized corrosion initiation of thin passive film is considered.

The results of the EDX analysis performed for the points indicated by numbers in Fig. 7C and Fig. 7D are given in Table 2. The EDX analysis of point 1 in the gray area of Fig. 7C provides a composition, which is quite close to the nominal composition of the material, thus it is related to the non-corroded sample surface. However, by EDX analysis the Nb signal could not be detected, which is suprising because although the Nb concentration is small, it should still be above the detection limit of EDX.

The points 2 and 3 located in the centre of a pit formed in 0.1 M HCl show a high enrichment of Cu inside the pit but no evidence of thick corrosion products on the surface. The EDX analysis of the outer region of the pit (point 4 in Fig. 7C) reveals an increased oxygen content, confirming the formation of corrosion products for this area. The EDX analysis performed on the corroded surface of Zr-BMG in 0.1 M NaCl provides similar results, *i.e.* enrichment of Cu in the centre of the pit (point 6 in Fig. 7D). Thus, the results of SEM-EDX analysis confirm the data achieved with the novel potentiostat hyphenated microflow-capillary FI-ICP-MS technique. A preferential active dissolution of less noble elements like Zr and Al and an enrichment of Cu inside the pits was also proposed for Zr-based bulk metallic glasses of different compositions, *e.g.* for $Zr_{50}Cu_{(40-x)}Al_{10}Pd_x$[32] or Cu–Zr metallic glasses.[33] The ICP-MS observation also points to the fact that the role of Zr is limited to its passivation properties. Thus, the data achieved with the novel potentiostat hyphenated microflow-capillary FI-ICP-MS technique clearly demonstrate a preferential dissolution of less noble elements like Ni and Al from Zr-BMG, whereas Cu release from the material is strongly hindered.

Conclusions

The novel potentiostat hyphenated microflow-capillary FI-ICP-MS technique offers distinct advantages over traditional separate electrochemical techniques or chemical bulk immersion tests by plasma spectrometry. Due to the hyphenation of the electrochemical instrument a control of the corrosion processes can be achieved. At the same time a simultaneous acquisition of electrochemical and online time- and element-resolved ICP-MS data allows a thorough online characterization of corrosion behaviour of an investigated material.

The efficiency of the hyphenated technique was demonstrated by analysis of the corrosion susceptibility of $Zr_{58.5}Cu_{15.6}Ni_{12.8}Al_{10.3}Nb_{2.8}$ in 0.1 M HCl, 0.1 M NaCl and 0.001 M NaCl solutions. The electrochemical and element-resolved corrosion behaviour was investigated during potentiodynamic polarization of the bulk metallic glass sample. The analysis revealed a very low dissolution of Al and Cu on a level of ng cm^{-2} in the cathodic domain. This finding is explained by a preferential process of Al and Cu dissolution from the oxide film as a result of alkalinisation at the sample surface. During the polarization of the sample, once the E_{pit} is reached, a massive release of all elements (with the exception of Cu) is detected in the range of μg cm^{-2} to mg cm^{-2}.

Acknowledgements

The authors gratefully acknowledge the Swiss National Science Foundation for the financial support of the project. NASAs Genesis curation team is acknowledged for providing the sample.

References

1 D. Beauchemin, *Analytical Chemistry*, 2008, **80**, 4455–4486.
2 N. Homazava, A. Ulrich, M. Trottmann and U. Krähenbühl, *Journal of Analytical Atomic Spectrometry*, 2007, **22**, 1122–1130.
3 A. Sarmiento-González, J. R. Encinar, J. M. Marchante-Gayón and A. Sanz-Medel, *Analytical and Bioanalytical Chemistry*, 2008, 1–9.
4 J. C. Rubio, M. C. Garcia-Alonso, C. Alonso, M. A. Alobera, C. Clemente, L. Munuera and M. L. Escudero, *Journal of Materials Science: Materials in Medicine*, 2008, **19**, 369–375.
5 S. Hochstrasser, Y. Mueller, C. Latkoczy, S. Virtanen and P. Schmutz, *Corrosion Science*, 2007, **49**, 2002–2020.
6 K. Ogle and S. Weber, *Journal of the Electrochemical Society*, 2000, **147**, 1770–1780.
7 D. Hamm, K. Ogle, C. O. Olsson, S. Weber and D. Landolt, *Corrosion Science*, 2002, **44**, 1443–1456.
8 K. Ogle, A. Tomandl, N. Meddahi and M. Wolpers, *Corrosion Science*, 2004, **46**, 979–995.
9 S. Hochstrasser-Kurz, D. Reiss, T. Suter, C. Latkoczy, D. Günther, S. Virtanen, P. J. Uggowitzer and P. Schmutz, *Journal of the Electrochemical Society*, 2008, **155**, C415–C426.
10 N. Homazava, A. Ulrich and U. Krähenbühl, *Spectrochimica Acta - Part B Atomic Spectroscopy*, 2008, **63**, 777–783.
11 N. Homazava, A. Ulrich and U. Krähenbühl, *Chimia*, 2008, **62**, 530.
12 T. Suter and H. Böhni, *Electrochimica Acta*, 1997, **42**, 3275–3280.
13 T. Suter and H. Böhni, *Electrochimica Acta*, 2001, **47**, 191–199.
14 T. Suter, P. Schmutz and O. V. Trzebiatowski, *ECS Transactions*, 2007, **3**, 29–37.

 This journal is © The Royal Society of Chemistry 2009

View Article Online

15 F. Eckermann, T. Suter, P. J. Uggowitzer, A. Afseth and P. Schmutz, *Electrochimica Acta*, 2008, **54**, 844–855.
16 W. H. Wang, C. Dong and C. H. Shek, *Materials Science and Engineering R: Reports*, 2004, **44**.
17 A. L. Greer and E. Ma, *MRS Bulletin*, 2007, **32**, 611–615.
18 S. Pang, T. Zhang, H. Kimura, K. Asami and A. Inoue, *Materials Transactions, JIM*, 2000, **41**, 1490–1494.
19 D. Zander and U. Köster, *Materials Science and Engineering A*, 2004, **375–377**, 53–59.
20 J. R. Scully, A. Gebert and J. H. Payer, *Journal of Materials Research*, 2007, **22**, 302–313.
21 D. Zander, B. Heisterkamp and I. Gallino, *Journal of Alloys and Compounds*, 2007, **434–435**, 234–236.
22 A. Grimberg, H. Baur, P. Bochsler, F. Bühler, D. S. Burnett, C. C. Hays, V. S. Heber, A. J. G. Jurewicz and R. Wieler, *Science*, 2006, **314**, 1133–1135.
23 N. Homazava, A. Shkabko, D. Logvinovich, U. Krähenbühl and A. Ulrich, *Intermetallics*, 2008, **16**, 1066–1072.
24 A. Gebert, K. Buchholz, A. Leonhard, K. Mummert, J. Eckert and L. Schultz, *Materials Science and Engineering A*, 1999, **267**, 294–300.
25 U. K. Mudali, S. Baunack, J. Eckert, L. Schultz and A. Gebert, *Journal of Alloys and Compounds*, 2004, **377**, 290–297.
26 S. K. Sharma, T. Strunskus, H. Ladebusch and F. Faupel, *Materials Science and Engineering A*, 2001, **304–306**, 747–752.
27 P. Vanysek in *Handbook of Chemistry and Physics* (74th ed.), ed. D. R. Lide, CRC Press, Boca Raton, 1993–1994.
28 C. Alquier, M. T. Vandenborre and M. Henry, *Journal of Non-Crystalline Solids*, 1986, **79**, 383–395.
29 A. S. Solovkin and Z. N. Tsvetkova, *Russ. Chem. Rev.*, 1962, **31**(11), 655–669.
30 P. Plagemann, *Untersuchungen zur Lochkorrosion von Kupferrohren in Trinkwasserinstallationen*, Dissertation, RWTH Aachen, 2001.
31 R. G. Buchheit, R. P. Grant, P. F. Hlava, B. McKenzie and G. L. Zender, *Journal of the Electrochemical Society*, 1997, **144**, 2621–2628.
32 B. A. Green, H. M. Meyer, R. S. Benson, Y. Yokoyama, P. K. Liaw and C. T. Liu, *Corrosion Science*, 2008, **50**, 1825–1832.
33 H. B. Lu, L. C. Zhang, A. Gebert and L. Schultz, *Journal of Alloys and Compounds*, 2008, **462**, 60–67.

Published on 27 April 2009. Downloaded by Michigan State University on 23/01/2016 09:10:25.